JCI The Journal of Clinical Investigation

RAB7 deficiency impairs pulmonary artery endothelial function and promotes pulmonary hypertension

Bryce Piper, … , David M. Eckmann, Laszlo Farkas

J Clin Invest. 2023. https://doi.org/10.1172/JCI169441.

Research In-Press Preview Pulmonology

Graphical abstract

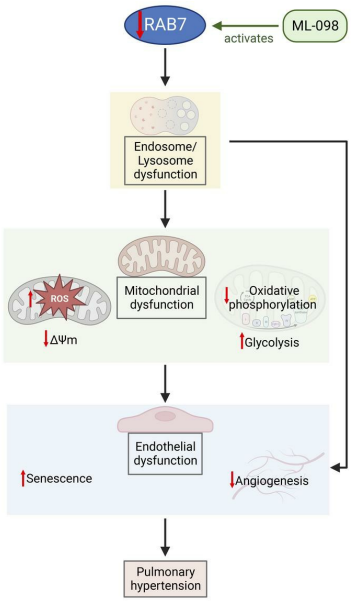

RAB7 deficiency impairs pulmonary artery endothelial function and promotes pulmonary hypertension

Bryce Piper[1, 2*], Srimathi Bogamuwa[1, 2*], Tanvir Hossain[3], Daniela Farkas[1, 2], Lorena Rosas[1, 2], Adam Green[3], Geoffrey Newcomb[1, 2], Nuo Sun[2, 4], Jose A. Ovando-Ricardez[1, 2], Jeffrey C. Horowitz[1, 2], Aneel R. Bhagwani[1, 2, 5], Hu Yang[6], Tatiana V. Kudryashova[7], Mauricio Rojas[1, 2], Ana L. Mora[1, 2], Pearlly Yan[8], Rama K. Mallampalli[1, 2], Elena A. Goncharova[9], David M. Eckmann[3, 10], Laszlo Farkas[1, 2]

* equal contribution

[1] Division of Pulmonary, Critical Care & Sleep Medicine, Department of Internal Medicine, The Ohio State University, Columbus, OH
[2] Davis Heart and Lung Research Institute, The Ohio State University, Columbus, OH
[3] Department of Anesthesiology, The Ohio State University, Columbus, OH
[4] Department of Cell Biology and Physiology, The Ohio State University, Columbus, OH
[5] Department of Physiology, Ziauddin University, Karachi, Pakistan
[6] Linda and Bipin Doshi Department of Chemical and Biochemical Engineering, Missouri University of Science and Technology, Rolla, MO
[7] University of Pittsburgh, Heart, Blood, and Vascular Medicine Institute, Pittsburgh, PA
[8] Division of Hematology, Department of Intern Medicine and The James Cancer Center, The Ohio State University, Columbus, OH
[9] Division of Pulmonary, Critical Care and Sleep Medicine, Department of Internal Medicine, University of California Davis, Davis, CA
[10] Center for Medical and Engineering Innovation, The Ohio State University, Columbus, OH

Corresponding author: Laszlo Farkas, MD
Division of Pulmonary, Critical Care and Sleep Medicine
Department of Internal Medicine
Davis Heart and Lung Research Institute
473 W 12th Avenue
Columbus, OH, 43210, USA
+1(614)-685-0555.
Laszlo.Farkas@osumc.edu

Conflict of Interest Statement: J.C.H. owns stock in Merck and Pfizer. The other authors declare no conflict of interest.

ABSTRACT

Pulmonary arterial hypertension (PAH) is a devastating and progressive disease with limited treatment options. Endothelial dysfunction plays a central role in the development and progression of PAH, yet the underlying mechanisms are incompletely understood. The endosome-lysosome system is important to maintain cellular health, and the small GTPase RAB7 regulates many functions of this system. Here, we explored the role of RAB7 in endothelial cell (EC) function and lung vascular homeostasis. We found reduced expression of RAB7 in ECs from PAH patients. Endothelial haploinsufficiency of RAB7 caused spontaneous PH in mice. Silencing of RAB7 in ECs induced broad changes in gene expression revealed via RNA sequencing, and RAB7 silenced ECs showed impaired angiogenesis, expansion of a senescent cell fraction, combined with impaired endolysosomal trafficking and degradation, suggesting inhibition of autophagy at the pre-degradation level. Further, mitochondrial membrane potential and oxidative phosphorylation were decreased, and glycolysis was enhanced. Treatment with the RAB7 activator ML-098 reduced established PH in chronic hypoxia/SU5416 rats. In conclusion, we demonstrate here for the first time the fundamental impairment of EC function by loss of RAB7, causing PH, and show RAB7 activation as a potential therapeutic strategy in a preclinical model of PH.

Word count: 195

INTRODUCTION

Pulmonary arterial hypertension (PAH) is a severe and fatal condition characterized by increased pulmonary artery pressure and extensive remodeling of all layers of the pulmonary artery wall (1, 2). The molecular pathogenesis of PAH remains incompletely understood at this time (1). One important and defining feature of pulmonary arterial dysfunction and remodeling in PAH is lung endothelial cell (EC) dysfunction. Following endothelial injury and apoptosis, endothelial dysfunction presents as unchecked proliferation likely following endothelial injury and apoptosis, impaired angiogenesis, enhanced release of pro-inflammatory cytokines, and upregulation of adhesion molecules (1). Similar to cancer, the hyperproliferative ECs in PAH may derive from clonal expansion of primitive stem-cell-like ECs (3, 4). Our previous work indicates also that while these primitive, hyperproliferative ECs can promote lung vascular remodeling, this remodeling is reversible after removal of additional triggers, such as hypoxia (4). This result indicates that proliferation alone may not be sufficient to develop progressive pulmonary vascular remodeling and PAH. Recently, a subpopulation of senescent ECs has been identified in pulmonary artery endothelial cells (PAECs) from patients with several forms of pulmonary hypertension (PH), including PAH, and these senescent ECs appear to promote the irreversibility of PA remodeling and PH (5, 6). We will use the term “PH” when describing animal models throughout the manuscript. The dysfunctional ECs from PAH patients further exhibit dysfunction of mitochondria, including dysregulation of mitochondrial membrane potential $\Delta\Psi_m$, reduced mitochondrial mass, impaired oxidative phosphorylation, and glycolytic shift akin to cancer cells (7-10). PAH ECs show reduced oxidative phosphorylation, but the impaired regulation of mitochondrial

health in PAH ECs is not sufficiently explained (8). Key cellular functions are regulated by autophagy, or the endolysosomal degradation of macromolecules and cell organelles, including mitochondria (11). In animal models of PH, conflicting results either attribute a protective function to physiologic autophagy or indicate that inhibition of aberrant autophagy is a treatment for PH (12, 13). Endosomal sorting, trafficking, and fusion of endosomes and lysosomes to endolysosomes are critical steps in physiologic autophagy (14). The small GTPase RAB7A has a key function in all these steps (15, 16). RAB7A is commonly referred to as RAB7, which we will use throughout the manuscript. Consequently, loss of RAB7 disrupts cellular function and impairs mitochondrial health, amplifying tissue injury (17-20).

We hypothesized that endothelial RAB7 deficiency is a cause of endothelial dysfunction in PAH through inhibition of autophagy on the pre-degradation level and promotes lung vascular remodeling and PH. We show here for the first time reduced RAB7 expression in PAECs from PAH patients and identified that endothelial-specific reduction of RAB7 expression caused spontaneous PH in mice. In vitro, RAB7 knockdown impaired endolysosomal trafficking and degradation and fundamentally altered gene expression in PAECs with functional evidence of impaired angiogenesis and expansion of a senescent EC subpopulation. In RAB7 deficient ECs, we detected the loss of $\Delta\Psi_m$ with a shift towards dysfunctional mitochondria and evidence of reduced mitochondrial respiration with enhanced glycolysis. The RAB7 GTPase activator ML-098 reduced severe PH in Hx/Su rats, hence supporting RAB7 as a potential therapeutic target in PAH.

RESULTS

Endosomal GTPase RAB7 is reduced in PAECs from patients with PAH.

We first identified the expression of RAB7 in lung tissues, PAECs, and pulmonary artery smooth muscle cells (PASMCs) from patients with PAH. The expression of RAB7 was reduced in vWF^+ PAECs in concentric and plexiform lesions from PAH patients compared to control lungs (**Figure 1A**). PAH PAECs had reduced expression of RAB7, whereas PAH PASMCs had similar RAB7 protein expression levels as control PAECs (**Figure 1, B and C**). The demographic information for the tissues and cell lines is in Supplemental Tables 1-3.

Endothelial RAB7 haploinsufficiency causes spontaneous PH.

We then studied RAB7 expression in the chronic hypoxia/SU5416 (Hx/Su) rat model of PH, because this model reproduces many features of PAH, including the occlusive pulmonary arteriopathy that is characteristic of PAH (21, 22). We found, using lung tissue sections and protein lysate, an overall reduction of RAB7 expression in the lung tissue of Hx/Su rats at days 21 and 42 and localized the reduction to the ECs in the remodeled pulmonary arteries of Hx/Su rats (**Figure 2, A and B**). Then, we generated heterozygous EC-specific *RAB7* knockout (KO, endothelial *RAB7* haploinsufficient) mice by crossbreeding $RAB7^{fl/fl}$ mice with Cdh5-Cre mice. We found increased media wall thickness (MWT) and right ventricular systolic pressure (RVSP) and a decreased ratio of pulmonary artery acceleration time /pulmonary ejection time (PAAT/PET) in $RAB7^{fl/wt}$ Cdh5-Cre^+ mice after exposure to Hx/Su, indicating exaggerated pulmonary artery remodeling and PH with endothelial *RAB7* haploinsufficiency (**Figure 2, C-G**).

Echocardiographically estimated right ventricular (RV) cardiac output was reduced in Hx/Su-exposed *RAB7*$^{fl/wt}$ Cdh5-Cre^{-} mice without difference between Cre^{-} and Cre^{+} mice (**Figure 2H**). Further evaluating the changes in the RV, we found that endothelial *RAB7* haploinsufficiency impaired the RV capillary density (**Supplemental Figure 1**) without affecting the RV hypertrophic response as measured by Fulton index and RV cardiomyocyte cross-sectional area (CM CSA) (**Figure 2E**, and **Supplemental Figure 2**). Further, we examined if endothelial *RAB7* haploinsufficiency promotes endothelial-to-mesenchymal transition (EnMT) in vivo. We analyzed the presence of ECs expressing the mesenchymal/smooth muscle cell marker α-smooth muscle actin (α-SMA) and of ECs with nuclear expression of the EnMT transcription factor SNAIL. While Hx/Su treatment increased the fraction of α-SMA^{+} ECs and SNAIL^{+} ECs, endothelial *RAB7* haploinsufficiency promoted endothelial SNAIL expression in pulmonary arteries following Hx/Su exposure, but not under normoxic conditions (**Supplemental Figure 3**).

Gene silencing of RAB7 induces endothelial dysfunction in PAECs.

We then tested if RAB7 expression contributes to physiological EC function. Using siRNA targeting of *RAB7* and bulk RNA sequencing (RNAseq), we found that *RAB7* knockdown resulted in differential expression of 4842 genes using analysis parameters of fold change >|1.25| and adjusted P value <0.05. We detected a substantial amount of differentially expressed genes (DEGs) with function in cell cycle and DNA repair, cellular movement and trafficking, immune function and inflammation, and development (**Figure 3**). Genes affecting angiogenesis and EC barrier function were among the DEGs with the highest n-fold changes in *RAB7* siRNA-treated PAECs. We found upregulation of anti-

angiogenic genes *PCDH17*, *IGFBP6* and *CH25H*, and downregulation of angiogenic and EC function genes *DLL4, UNC5B, CLDN5, RASIP1, PGF, GJA5, EPN3, CCM2L and TSPAN18* (**Figure 4A**). We then tested EC function in vitro and found that knockdown of *RAB7* inhibited angiogenic network formation and gap closure, indicating impaired migration (**Figure 4, B, and C**). Consistent with these functional changes, our RNAseq data revealed a pro-senescent transcriptomic signature in *RAB7* siRNA-treated PAECs (**Figure 4D**). These findings were mirrored by elevated p16 protein level (**Figure 4E**) and increased fraction of senescence-associated β-galactosidase (SA-β-gal)$^{+}$ PAECs (**Figure 4F**). We then tested the potential role of RAB7 deficiency in EnMT in vitro. *RAB7* knockdown induced activation of Ingenuity pathways that promote fibrotic remodeling and EnMT (**Supplemental Figure 4A**). In addition, some changes in mRNA supported an EnMT phenotype, as shown by the reduction of mRNA of Cadherin 5 (*CDH5)* and elevation of Transgelin (*TAGLN)* (**Supplemental Figure 4B**). At the protein level, the key finding was the downregulation of platelet endothelial cell adhesion molecule 1 (PECAM1), a marker of ECs. We did, however, not observe a concurrent upregulation of proteins typically associated with vascular smooth muscle cells, such as α-SMA, CALPONIN 1, and SM-22α (TAGLN). Furthermore, our analysis did not reveal a statistically significant upregulation of snail family transcriptional repressor 1 (SNAIL), a transcription factor often implicated in the regulation of EnMT (**Supplemental Figure 4**, **C-E**).

RAB7 is required for endolysosome function in PAECs.

Endolysosome function requires RAB7 (15, 23-25). To identify the extent to which RAB7 is required for endolysosome function in PAECs, we studied intracellular endolysosome trafficking in PAECs from PAH patients and in control PAECs following *RAB7* knockdown. Using pHrodo dextran, which emits fluorescence after acidification in endosome and lysosome, we detected that dextran accumulates in PAH PAECs in enlarged vesicles (**Figure 5A**). Using baculovirus-mediated expression of the GFP-labeled RAB5A, a marker of the early endosome, we found that pHrodo dextran accumulates in enlarged RAB5A^{+} early endosomes following endosomal uptake in *RAB7*-silenced PAECs (**Figure 5B**). *RAB7* siRNA also caused the accumulation of pHrodo dextran in enlarged lysosomes, which we detected by staining with lysotracker (**Figure 5C**). Consistently, our RNAseq data revealed the downregulation of multiple autophagy-related genes with *RAB7* siRNA (**Figure 5D**). Reduced cathepsin B activity further supported reduced lysosomal autophagy in *RAB7*-silenced PAECs (**Figure 5E**).

RAB7 knockdown impairs mitochondrial membrane potential and oxidative phosphorylation.

Because autophagy is important to maintain physiologic mitochondrial function (26), we tested the role of RAB7 in the maintenance of the mitochondrial membrane potential $\Delta\Psi_m$ and mitochondrial respiration. Using a flow cytometry assay for TMRE Tetramethylrhodamine ethyl ester (TMRE) and mitotracker green, we found that *RAB7* knockdown reduced the fraction of ECs with functional mitochondria (polarized) while increasing the fraction of ECs with dysfunctional (depolarized) mitochondria, indicating an overall reduction in $\Delta\Psi_m$ (**Figure 6A**). Using fluorescence microscopy of

Tetramethylrhodamine methyl ester (TMRM) staining, *RAB7* silencing caused a net reduction in $\Delta\Psi_m$ with accumulation of the remaining functional mitochondria in the perinuclear region (**Figure 6B**). We further detected increased mitochondrial net motility in perinuclear and peripheral regions in *RAB7* siRNA PAECs (**Figure 6B**). *RAB7* silencing also increased mitochondrial production of reactive oxygen species (ROS) as measured by mitoSOX flow cytometry assay (**Figure 6C**). RNAseq analysis of PAECs treated with *RAB7* siRNA revealed upregulation of mRNA for multiple genes related to glycolysis, whereas the mRNA of various genes related to oxidative phosphorylation was reduced (**Figure 6D**). *RAB7* knockdown also impaired oxidative phosphorylation because our data show reduced oxygen consumption rate (OCR) at baseline, maximal respiration, and spare respiratory capacity (**Figure 6E**). There was no difference in proton leak. In addition, *RAB7* siRNA-treated PAECs had higher lactate production than control siRNA-treated PAECs, indicating a shift toward glycolysis (**Figure 6F**). Lastly, the extracellular acidification rate (ECAR) measurements revealed increased glycolysis, glycolytic capacity, and glycolytic reserve (**Figure 6G**).

RAB7 activator ML-098 reduces experimental PH in rats.

To aid translation of our findings to a potential treatment option, we tested if the RAB7 GTPase activator ML-098 reduces experimental PH induced by Hx/Su in rats. First, we performed a preventive dose-response experiment (day 1-21) to find the lowest efficacious dose. We found overall that 1.0 and 10 mg/kg doses reduced pulmonary artery occlusion, MWT, and RVSP most effectively and successfully increased PAAT/PET and cardiac output, which were obtained by echocardiography (**Supplemental Figure 5**).

Based on these results, we opted for 1.0 mg/kg in the interventional treatment approach (day 22-35). In this approach, ML-098 treatment reduced RVSP, Fulton index, MWT, pulmonary artery occlusion, and mural cell proliferation while increasing PAAT/PET, tricuspid annular plane systolic excursion (TAPSE), and cardiac output (**Figure 7**). In addition, our data also demonstrate a reduction in EnMT in the pulmonary arteries of Hx/Su rats treated with ML-098 compared to vehicle-treated Hx/Su rats by reduction of the fraction of α-SMA$^+$ ECs and SNAIL$^+$ ECs in the pulmonary arteries (**Supplemental Figure 6**). The results from the interventional treatment were further supported by our data from a reversal treatment approach with ML-098 (day 36-49): This treatment regimen resulted in reduction of RVSP, Fulton index, MWT, pulmonary artery occlusion, mural cell proliferation, and in increase in PAAT/PET, TAPSE and cardiac output (**Figure 8**). Hence, the RAB7 GTPase activator ML-098 prevents and reduces occlusive pulmonary artery remodeling, EnMT, PH and RV dysfunction induced by Hx/Su.

DISCUSSION

PAH remains a deadly disease and current vasodilator therapies are not sufficient to cure the disease by a lack of effect on the progressive occlusive pulmonary arteriopathy that is a hallmark of PAH (1, 2). One potential underlying cause is that these treatments mainly improve the vasotonus function of ECs but not the overall EC dysfunction (1, 2). As coordinated autophagy and mitochondrial function have been shown to be important drivers of physiologic EC function (7-11), we sought to find a unifying pathogenetic process that explains these findings. The endosome-lysosome system holds a key role in the trafficking, recycling, and degradation of macromolecules and cell organelles, such

as mitochondria. The GTPase RAB7 is crucial for regulating endosome-lysosome function, autophagy, and cell function. Hence, we hypothesized that endothelial RAB7 deficiency is a cause of endothelial dysfunction, lung vascular remodeling, and PAH.

The main findings of our study are that 1) PAECs from PAH patients have reduced RAB7 expression and impaired endosome-lysosome function; 2) endothelial haploinsufficiency of *RAB7* induces spontaneous PH; 3) Silencing of *RAB7* in human PAECs impairs endosome/lysosome function, autophagy, and angiogenesis, and promotes cellular senescence; 4) RAB7 insufficiency reduced mitochondrial membrane potential $\Delta\Psi_m$ and oxidative phosphorylation while promoting mitochondrial ROS production and glycolysis; 5) The RAB7 GTPase activator ML-098 reduced severe PH and right heart dysfunction induced by cHx/Su.

Whereas all layers of the pulmonary artery wall and all mural cell types are affected, EC dysfunction has emerged as one of the key drivers of pulmonary artery remodeling in PAH (27). ECs not only provide an important barrier but in the pulmonary circulation also affect smooth muscle cell function by regulation of, e.g., vasotonus or smooth muscle cell growth through the release of mediators (27). In addition, altered EC function may contribute to lung vascular remodeling by microvascular dropout following EC apoptosis and to the development of complex plexiform lesions through aberrant cell growth (4, 28-30). Yet current therapeutic avenues are unsuccessful in restoring physiologic EC function and reversing pulmonary artery remodeling.

Endosomes develop as plasma membrane invaginations during endocytosis and are a shuttle for macromolecules from the outside of the cell into the cell (31). In addition, the internalization of receptors and other macromolecules from the cell membrane occurs

also through the endosome system. After initial formation, endosomes are designated “early endosomes” and carry specific surface molecules, including early endosome antigen 1 (EEA1) and members of the RAB family of small GTPases, such as RAB5 (31, 32). During sorting, endosomal content, including macromolecules and cell organelles, is either recycled to the cell surface or designated for degradation via autophagy. Upon maturation to multivesicular “late endosomes”, these fuse with lysosomes to endolysosomes as sites of autophagy (31). RAB7 is a GTPase with a central function in endosomal sorting, trafficking, and fusion with lysosomes (31). Not surprisingly, loss of RAB7 impairs autophagy and particularly autophagy of mitochondria, or mitophagy, and hence cell function (15, 18-20, 33-37). Our results show that PAECs, but not PASMCs, from patients with PAH have reduced expression of RAB7 and impaired endosomal trafficking and/or degradation of dextran. Consequently, endothelial *RAB7* haploinsufficient mice developed spontaneous PH under normoxic conditions and more severe PH following exposure to Hx/Su, suggesting a fundamental protective role for physiologic levels of RAB7 in PAECs. Our results further show that *RAB7* silencing in PAECs impairs endosomal and lysosomal trafficking and/or degradation, indicating that RAB7 is essential for autophagy. While knockout of the autophagy component Microtubule-associated proteins 1A/1B light chain 3B (LC3B) promoted PH in a mouse model and supports our findings, some studies have hinted at a potential role for excessive autophagy in EC dysfunction and PH progression (12, 13, 38, 39). A more detailed analysis of endosome/lysosome function and degradation processes in ECs and other vascular cell types will likely be required to reveal a definitive answer.

Our focus here was on elucidating the functional role of RAB7 in PAECs, and evidence is accumulating that mitochondrial dysfunction has a central role in regulating EC dysfunction and pulmonary artery remodeling (7, 9, 10, 40). RAB7 is a known modulator of mitochondrial health through mitochondrial fission and mitophagy, and we found that knockdown of *RAB7* reduces mitochondrial membrane potential $\Delta\Psi_m$ and impairs oxidative phosphorylation. These findings are consistent with enhanced glycolysis and lactate production, as well as impaired clearance of mitochondrial ROS. Impaired mitochondrial respiration and a shift towards glycolysis are all known features of PAECs from PAH patients and are consistent with dysregulation of EC function akin to a “Warburg effect” (7, 9, 10). Increased mitochondrial ROS has been previously shown in bone morphogenic protein receptor 2 (BMPR2) knockout ECs, and reduced $\Delta\Psi_m$ was caused in PAH PAECs by hypoxia-reoxygenation but not by normoxia exposure (9). Hence, our findings corroborate that RAB7 deficiency contributes to impaired mitochondrial health and function in PAH PAECs.

Our results further show that silencing of RAB7 impairs angiogenesis and migration in PAECs and promotes senescence in PAECs. Impaired angiogenesis has been previously shown in PAECs and late outgrowth endothelial progenitor cells from PAH patients (41, 42). While these studies focused on the proliferative phenotype of PAH PAECs, more recent studies have demonstrated that endothelial senescence is also present in PAH PAECs and contributes to endothelial dysfunction and the progressive nature of pulmonary artery remodeling (5, 6). Our findings further show that *RAB7* knockdown affected transcription of gene clusters affecting organ and tissue survival, cell death, cell growth and inflammatory, developmental and immune response. The

angiogenic deficit and senescence also show in the transcriptomic profile of *RAB7* silenced PAECs. Because of its fundamental function in endosome and lysosome function and autophagy/mitophagy, we show in our work that endothelial RAB7 has an important protective function in the pulmonary vasculature. One additional important aspect of endothelial dysfunction in PAH is EnMT (43-45). *RAB7* knockdown promoted in vitro the transcriptomic activation of pathways for fibrotic remodeling and EnMT. Our findings suggest that while we were able to detect a consistent downregulation of the endothelial marker PECAM1 in vitro, this decrease was not accompanied by upregulation of smooth muscle cell-specific genes and the EnMT transcription factor SNAIL. In contrast, *RAB7* knockdown can promote the upregulation of SNAIL in HUVECs (46). We found in vivo that endothelial RAB7 deficiency only exaggerated pulmonary artery endothelial SNAIL expression in Hx/Su exposed but not in normoxia-treated mice. This suggests that the regulation of SNAIL in the context of pulmonary arterial endothelial RAB7 deficiency cannot be modeled in monocultures.

Further, we also found that endothelial *RAB7* haploinsufficiency impaired RV capillary density, further confirming the important role of RAB7 in vascular integrity. Yet little is known regarding the regulation of RAB7 expression in lung ECs. In other organs and cancer cells, multiple transcription factors have been shown to regulate RAB7 transcription, including Forkhead box protein O1 (FoxO1), c-myc, and, under hypoxia exposure, signal transducer and activator of transcription 3 (STAT3) (47-49). Among these, hypoxia and STAT3 signaling are enhanced in ECs from PAH patients (7) and repress RAB7 expression in ovarian cancer cells (48), suggesting that hypoxia and STAT3 signaling may contribute to RAB7 deficiency in ECs from PAH patients.

To determine if enhancing the activity of remaining RAB7 provides a therapeutic avenue, we used the GTPase activator ML-098, which has a low ED_{50} for RAB7 and a much smaller affinity to other small GTPases (50). Our study was the first to use ML-098 in in vivo experiments. According to our findings, ML-098 treatment not only prevented but also reduced established PH in rats exposed to Hx/Su. ML-098 has only been used in cell culture experiments, and authors have shown protection from age-related deterioration of oocytes (19), consistent with our observation that loss of RAB7 promotes senescence.

Our study has limitations: 1. Our work focused on the role of RAB7 in EC function and lung vascular remodeling, but other aspects of RAB7 deficiency, such as an exaggerated inflammatory response, may also be mechanistically relevant. 2. We have tested ML-098 only in the Hx/Su model of PH, although this is one of the most relevant models mimicking many features of PAH, including the progressive nature of the condition and the occlusive pulmonary arteriopathy (22, 51).

Taken together, we demonstrate in PAECs a fundamental role for the endolysosomal GTPase RAB7 in physiologic cell function, transcriptomic profile, endolysosome function, mitochondrial health, and pulmonary vascular integrity. Pharmacologic modulation of RAB7 function could complement existing therapeutic strategies and offer a new therapeutic avenue for patients with PAH.

METHODS

Reagents and constructs

Cell lines

Primary human pulmonary artery ECs (PAECs) and pulmonary artery smooth muscle cells (PASMCs) from male and female PAH and control patients (failed donors, no known pulmonary vascular disease) were obtained from the Pulmonary Hypertension Breakthrough Initiative (PHBI) and Cell Processing Cores at the University of Pittsburgh and University of California Davis. De-identified human primary cell lines were deemed "non-human subjects research" by the Office of Research Subjects Protection at OSU.

Tissue samples

De-identified Formalin-fixed, paraffin-embedded 5 μm tissue sections were obtained from the Pulmonary Hypertension Breakthrough Initiative (PHBI). De-identified human tissue samples were deemed "non-human subjects research" by the Office of Research Subjects Protection at OSU.

Animal models:

RAB7$^{fl/wt}$Cdh5-Cre mice were generated by crossbreeding *RAB7*$^{fl/fl}$ mice (52) [strain B6.129(Cg)-*Rab7*$^{tm1.1Ale}$/J, #021589, Jackson Labs, Bar Harbor, ME] with vascular endothelial cadherin (VE-cadherin, *Cdh5*) Cre mice (53) [strain B6.Cg-Tg(Cdh5-cre)1Spe/J, #033055, Jackson Labs]. *RAB7*$^{fl/fl}$ mice and Cdh5-Cre mice are on a C57BL/6J background. The mice used in the experiments were crossbred for at least 5 generations. Male and female mice aged 8-16 weeks were used for the experiments.

Genotyping was performed by Transnetyx (Cordova, TN). Littermate *RAB7*$^{fl/wt}$Cdh5-Cre^{-} mice were used as controls in the experiments. For rat experiments, male Sprague Dawley rats (Hsd:Sprague Dawley® SD®) were obtained from Inotiv (Indianapolis, IN) at the age of 6 weeks.

Animal experiments

For the chronic hypoxia + SU5416 (Hx/Su) rat model, 6-week-old male rats were treated with SU5416 s.c. (20 mg/kg body weight, Millipore Sigma, S8442) at the beginning of 3 weeks of chronic hypoxia exposure (inspiratory oxygen fraction 10%) in a normobaric nitrogen dilution chamber (Biospherix), as published previously (54). For the Hx/Su mouse model, mice were given 20 mg/kg SU5416 s.c. once a week during a 3-week exposure to chronic hypoxia (54). ML-098 (TargetMol, T4619) was diluted in dimethyl sulfoxide (DMSO) and given to male rats after dilution in 0.9% saline (final 1% DMSO) at 0.1, 1.0 and 10 mg/kg body weight five times a week from day 1-21 (preventive) during the chronic hypoxia phase of the Hx/Su model or after return to normoxia from day 22-35 or day 36-49. For all treatments, animals were randomly assigned to the treatment groups, and treatments were given in a blinded manner. At the indicated time points, echocardiography was performed using a Vevo 2100 system (Visual Sonics, Toronto, ON, Canada) located at the Small Animal Imaging Facility at OSU or a GE Vivid IQ Premium system (GE Healthcare, Chicago, IL) under isoflurane anesthesia (rats) or under ketamine/xylazine anesthesia (mice). Echocardiographic estimation of the cardiac output was calculated according to (55). Terminal right heart catheterization was done with a 1.4F Millar catheter and Powerlab acquisition system (AD Instruments). For this

procedure, the animals were anesthetized with ketamine/xylazine and ventilated after tracheostomy with a small animal ventilator (RoVent, Kent Scientific Corporation). A median sternotomy was used to open the chest cavity, and the 1.4F Millar catheter was inserted following a small puncture of the right ventricle. Right ventricular hemodynamics were recorded over at least 5 min for steady-state measurements. Acquisition and analysis of echocardiographic and hemodynamic data was blinded by numerical coding.

Cell culture experiments

Human PAECs were cultured in complete endothelial growth medium-2 microvascular (EGM-2MV, Lonza, CC-3162) in a cell culture incubator at 37°C with 5% CO_2 and 100% humidity. Human PASMCs were cultured in complete smooth muscle cell growth medium-2 (SmGM-2, Lonza, CC-3182). For siRNA-mediated knockdown of RAB7, PAECs were transfected with 50 nM *RAB7* or control siRNA using GenMute Reagent (SL100568, SignaGen). The following siRNAs were used: RAB7 siRNA (IDT, NM_004637 13.2) and control siRNA (IDT, 51-01-14-04). After 24h, siRNA was removed, and experiments were performed at 48h or 72h after transfection. To test 2D angiogenic network formation, cells were seeded on Matrigel in µ-slide 15 well (Ibidi, 81506), and images of network formation were acquired at 4× magnification using an EVOS M7000 (ThermoFisher, AMF7000) automatic microscope. The images were analyzed using AngioTool software (NCI). To test gap closure, ECs were seeded in 3 well migration assay culture inserts (Ibidi, 80369). Removal of the insert left a well-defined uniform gap and gap closure was observed after 16h as published previously (54). To detect cellular senescence, cells were stained with senescence-associated (SA)-β-galactosidase (gal)

according to the manufacturer's instructions for Senescence β-galactosidase Staining Kit (Cell signaling, 9860). Cells were counterstained with DAPI. SA-β-gal activity was determined by the detection of blue-green precipitate over the cells. Cells were viewed using an EVOS M7000 automated fluorescence microscope (Invitrogen) under bright field illumination. To evaluate vesicular trafficking and degradation, cells were incubated with pHrodo™ Red dextran (P10361, Invitrogen) for 20 min, followed by fixation with 10% formalin. To specifically determine endosomal localization of dextran, GFP-conjugated RAB5A (early endosome marker) was expressed using a BacMam 2.0 baculovirus construct using the CellLight™ Early Endosomes-GFP kit (ThermoFisher, C10586. To obtain the lysosomal localization of dextran, lysosomes were stained with lysotracker green (ThermoFisher, L7526). To measure lysosome activity, a cathepsin B activity assay was used according to the manufacturer's recommendations (Cathepsin B assay kit, Promocell, PK-CA577-K140). To test mitochondrial membrane potential, we used the TMRE staining kit (200 nM) (Abcam, ab113852) combined with MitoTracker™ Green (mitogreen, 100 nM) (ThermoFisher, M7514) staining. Staining was performed in fetal calf serum-free media for 30 min. Carbonyl cyanide p-trifluoro methoxyphenylhydrazone (FCCP, included in TMRE staining kit) was added 10 min before staining at 20 μM. Analysis was performed using a BD FACSSymphony A1 flow cytometer and FlowJo 10 software (FlowJo). Data were presented as fractions of $TMRE^{high}$ $mitogreen^{high}$ (physiologic ΔΨm) and $TMRE^{low}$ $mitogreen^{high}$ cells (decreased $\Delta\Psi_m$). $\Delta\Psi_m$ distribution was also determined using TMRM staining (TMRM assay kit, Abcam, ab228569) on adherent PAECs followed by nuclear staining with Hoechst 33342 (ThermoFisher, H-1399). To determine mitochondrial ROS production, cells were stained with 2 μM

mitoSOX mitochondrial ROS staining (mitoSOX™ Red, ThermoFisher, M36008) for 20 min. combined with LIVE/DEAD™ Fixable Near-IR Dead Cell Stain Kit (ThermoFisher L34975), followed by analysis on BD FACSSymphony A1 flow cytometer and FlowJo 10 software. Lactate production was measured with the Lactate-Glo™ Assay (Promega, J5021) according to the manufacturer's recommendations.

Details regarding determining mitochondrial dynamics, Seahorse OCR/ECAR measurements, protein isolation, immunoblotting, RNA isolation, bulk RNA sequencing, histology, immunohistochemistry, and Microscopy are found in the Online Supplement.

Graphical abstract

The graphical abstract was drawn using BioRender (BioRender.com).

Statistical analysis

The normal distribution of data was tested with the D'Agostino-Pearson or Shapiro-Wilk test. Normally distributed data were shown as single data points and mean ± SD and were compared using 2-tailed Student's t-test (2 groups) or one or two-way ANOVA (more than 2 groups), followed by multiple comparison corrections using the Holm-Sidak or Sidak tests. Data that were not normally distributed were presented as median ± interquartile rank and were compared using non-parametric 2-tailed Mann-Whitney test (2 groups) or Kruskal-Wallis test (more than 2 groups), followed by Dunn's multiple comparison test. If 2 variables were analyzed, a 2-way ANOVA was used if the residual distribution was normally distributed. If residuals were not normally distributed, a Kruskal-

Wallis analysis was used to compare the outcome distribution between the groups. The calculations were performed using Prism 9.0 (GraphPad Software Inc., San Diego, CA). A P value of <0.05 was considered significant.

Study approval

De-identified human tissue samples and cell lines were deemed “non-human subjects research” by the Office of Research Subjects Protection at The Ohio State University (OSU). The PAECs and PASMCs were isolated in a de-identified manner under PHBI-approved protocols with institutional ethics board approval in accordance with the revised ethical guidelines of the Declaration of Helsinki of 1983. Informed consent was waived by these institutional review boards. Animal experiments were approved by the IACUC at OSU under protocol number 2019A00000092.

Data availability

Values for all data points in graphs are reported in the Supporting Data Values file. Original uncropped Western blots are included in the Supplemental Data file. Raw data files from bulk RNAseq data have been deposited to Gene Expression Omnibus (Accession number GSE243774). Data can also be obtained from the corresponding author upon request.

AUTHOR CONTRIBUTIONS

B.P., S.B., N.S., A.R.B., H.Y., R.K.M., E.A.G., D.M.E., and L.F. conceived and designed the study; B.P., S.B., T.H., D.F., L.R., A.G., G.N., J.A.O., A.R.B., T.V.K., P.Y., D.E.M. and L.F. performed experiments, obtained and analyzed data; B.P., S.B., D.M.E. and L.F. wrote the initial draft of the manuscript; all authors contributed to manuscript revision; all authors approved the final version; the order of co-first authors was based on the overall contribution to data acquisition and manuscript preparation.

ACKNOWLEDGEMENTS

The authors thank Dr. Jing Peng, The Ohio State University, for biostatistical advice. The authors further acknowledge the expert technical help of Dr. Mehboob Ali, Kyle Shin, Alexander Pan, Jaylen Hudson, Pranav Gunturu, and Dania Abu-Saleh. The study was supported by grants from the NIH/NHLBI (HL139881) to L.F., (HL130261, HL113178, HL159638, and HL103455) to E.A.G, and (HL166932) to T.V.K. The study was further supported by a grant from the Office of Naval Research Grant (ONR) N000142212170 to D.M.E. Data/Tissue samples provided by PHBI under the Pulmonary Hypertension Breakthrough Initiative (PHBI). Funding for the PHBI is provided under an NHLBI R24 grant, R24HL123767, and by the Cardiovascular Medical Research and Education Fund (CMREF). The authors acknowledge resources for confocal microscopy from the Campus Microscopy and Imaging Facility (CMIF), and the OSU Comprehensive Cancer Center (OSUCCC) Microscopy Shared Resource (MSR) at the Ohio State University with NIH S10 OD025008 and NIH NIC P30CA016058. Echocardiography was, in part, performed in the Small Animal Imaging Core at OSU. These facilities are

supported in part by grant P30 CA016058, National Cancer Institute, Bethesda, MD. RNA sequencing was performed in the Genomic Shared Resource of the OSU Comprehensive Cancer Center, partially supported by grant P30-CA016058 from the National Cancer Institute. The content is solely the responsibility of the authors and does not necessarily represent the official views of the National Institutes of Health.

References

1. Humbert M, Guignabert C, Bonnet S, Dorfmüller P, Klinger J, Nicolls M, et al. Pathology and pathobiology of pulmonary hypertension: state of the art and research perspectives. *Eur Respir J.* 2019;53(1).
2. Stacher E, Graham B, Hunt J, Gandjeva A, Groshong S, McLaughlin V, et al. Modern age pathology of pulmonary arterial hypertension. *Am J Respir Crit Care Med.* 2012;186(3):261-72.
3. Lee SD, Shroyer KR, Markham NE, Cool CD, Voelkel NF, and Tuder RM. Monoclonal endothelial cell proliferation is present in primary but not secondary pulmonary hypertension. *J Clin Invest.* 1998;101(5):927-34.
4. Bhagwani A, Farkas D, Harmon B, Authelet K, Cool C, Kolb M, et al. Clonally selected primitive endothelial cells promote occlusive pulmonary arteriopathy and severe pulmonary hypertension in rats exposed to chronic hypoxia. *Sci Rep.* 2020;10(1):1136.
5. Culley MK, Zhao J, Tai YY, Tang Y, Perk D, Negi V, et al. Frataxin deficiency promotes endothelial senescence in pulmonary hypertension. *J Clin Invest.* 2021;131(11).
6. van der Feen DE, Bossers GPL, Hagdorn QAJ, Moonen J-R, Kurakula K, Szulcek R, et al. Cellular senescence impairs the reversibility of pulmonary arterial hypertension. *Science Translational Medicine.* 2020;12(554):eaaw4974.
7. Fijalkowska I, Xu W, Comhair S, Janocha A, Mavrakis L, Krishnamachary B, et al. Hypoxia inducible-factor1alpha regulates the metabolic shift of pulmonary hypertensive endothelial cells. *Am J Pathol.* 2010;176(3):1130-8.
8. Xu W, Koeck T, Lara A, Neumann D, DiFilippo F, Koo M, et al. Alterations of cellular bioenergetics in pulmonary artery endothelial cells. *Proc Natl Acad Sci U S A.* 2007;104(4):1342-7.
9. Diebold I, Hennigs J, Miyagawa K, Li C, Nickel N, Kaschwich M, et al. BMPR2 preserves mitochondrial function and DNA during reoxygenation to promote endothelial cell survival and reverse pulmonary hypertension. *Cell Metab.* 2015;21(4):596-608.
10. Yu Q, Tai Y, Tang Y, Zhao J, Negi V, Culley M, et al. BOLA (BolA Family Member 3) Deficiency Controls Endothelial Metabolism and Glycine Homeostasis in Pulmonary Hypertension. *Circulation.* 2019;139(19):2238-55.
11. Ballabio A, and Bonifacino JS. Lysosomes as dynamic regulators of cell and organismal homeostasis. *Nat Rev Mol Cell Biol.* 2020;21(2):101-18.
12. Long L, Yang X, Southwood M, Lu J, Marciniak S, Dunmore B, et al. Chloroquine prevents progression of experimental pulmonary hypertension via inhibition of autophagy and lysosomal bone morphogenetic protein type II receptor degradation. *Circ Res.* 2013;112(8):1159-70.
13. Lee S, Smith A, Guo L, Alastalo T, Li M, Sawada H, et al. Autophagic protein LC3B confers resistance against hypoxia-induced pulmonary hypertension. *Am J Respir Crit Care Med.* 2011;183(5):649-58.
14. Chichger H, Rounds S, and Harrington E. Endosomes and Autophagy: Regulators of Pulmonary Endothelial Cell Homeostasis in Health and Disease. *Antioxid Redox Signal.* 2019;31(13):994-1008.

15. Girard E, Chmiest D, Fournier N, Johannes L, Paul J, Vedie B, et al. Rab7 is functionally required for selective cargo sorting at the early endosome. *Traffic.* 2014;15(3):309-26.
16. Guerra F, and Bucci C. Multiple Roles of the Small GTPase Rab7. *Cells.* 2016;5(3):34.
17. Cioni J, Lin J, Holtermann A, Koppers M, Jakobs M, Azizi A, et al. Late Endosomes Act as mRNA Translation Platforms and Sustain Mitochondria in Axons. *Cell.* 2019;176(1-2):56-72.e15.
18. Heo J, Ordureau A, Swarup S, Paulo J, Shen K, Sabatini D, et al. RAB7A phosphorylation by TBK1 promotes mitophagy via the PINK-PARKIN pathway. *Sci Adv.* 2018;4(11):eaav0443.
19. Jin X, Wang K, Wang L, Liu W, Zhang C, Qiu Y, et al. RAB7 activity is required for the regulation of mitophagy in oocyte meiosis and oocyte quality control during ovarian aging. *Autophagy.* 2021:1-18.
20. Takahashi K, Mashima H, Miura K, Maeda D, Goto A, Goto T, et al. Disruption of Small GTPase Rab7 Exacerbates the Severity of Acute Pancreatitis in Experimental Mouse Models. *Scientific Reports.* 2017;7(1):2817.
21. Taraseviciene-Stewart L, Kasahara Y, Alger L, Hirth P, Mc Mahon G, Waltenberger J, et al. Inhibition of the VEGF receptor 2 combined with chronic hypoxia causes cell death-dependent pulmonary endothelial cell proliferation and severe pulmonary hypertension. *FASEB J.* 2001;15(2):427-38.
22. Abe K, Toba M, Alzoubi A, Ito M, Fagan K, Cool C, et al. Formation of plexiform lesions in experimental severe pulmonary arterial hypertension. *Circulation.* 2010;121(25):2747-54.
23. Vanlandingham P, and Ceresa B. Rab7 regulates late endocytic trafficking downstream of multivesicular body biogenesis and cargo sequestration. *J Biol Chem.* 2009;284(18):12110-24.
24. Langemeyer L, Fröhlich F, and Ungermann C. Rab GTPase Function in Endosome and Lysosome Biogenesis. *Trends Cell Biol.* 2018;28(11):957-70.
25. Mrakovic A, Kay J, Furuya W, Brumell J, and Botelho R. Rab7 and Arl8 GTPases are necessary for lysosome tubulation in macrophages. *Traffic.* 2012;13(12):1667-79.
26. Pickles S, Vigié P, and Youle RJ. Mitophagy and Quality Control Mechanisms in Mitochondrial Maintenance. *Current Biology.* 2018;28(4):R170-R85.
27. Evans CE, Cober ND, Dai Z, Stewart DJ, and Zhao YY. Endothelial cells in the pathogenesis of pulmonary arterial hypertension. *Eur Respir J.* 2021;58(3):2003957.
28. Sakao S, Taraseviciene-Stewart L, Lee JD, Wood K, Cool CD, and Voelkel NF. Initial apoptosis is followed by increased proliferation of apoptosis-resistant endothelial cells. *FASEB J.* 2005;19(9):1178-80.
29. Teichert-Kuliszewska K, Kutryk M, Kuliszewski M, Karoubi G, Courtman D, Zucco L, et al. Bone morphogenetic protein receptor-2 signaling promotes pulmonary arterial endothelial cell survival: implications for loss-of-function mutations in the pathogenesis of pulmonary hypertension. *Circ Res.* 2006;98(2):209-17.

30. Farkas L, Farkas D, Ask K, Möller A, Gauldie J, Margetts P, et al. VEGF ameliorates pulmonary hypertension through inhibition of endothelial apoptosis in experimental lung fibrosis in rats. *J Clin Invest.* 2009;119(5):1298-311.
31. Brooks D. The endosomal network. *Int J Clin Pharmacol Ther.* 2009;47 Suppl 1:S9-17.
32. Zerial M, and McBride H. Rab proteins as membrane organizers. *Nature Reviews Molecular Cell Biology.* 2001;2:107-17.
33. Hida T, Sohma H, Kokai Y, Kawakami A, Hirosaki K, Okura M, et al. Rab7 is a critical mediator in vesicular transport of tyrosinase-related protein 1 in melanocytes. *J Dermatol.* 2011;38(5):432-41.
34. Kuchitsu Y, and Fukuda M. Revisiting Rab7 Functions in Mammalian Autophagy: Rab7 Knockout Studies. *Cells.* 2018;7(11):215.
35. Margiotta A, Progida C, Bakke O, and Bucci C. Rab7a regulates cell migration through Rac1 and vimentin. *Biochim Biophys Acta Mol Cell Res.* 2017;1864(2):367-81.
36. Takeda M, Koseki J, Takahashi H, Miyoshi N, Nishida N, Nishimura J, et al. Disruption of Endolysosomal RAB5/7 Efficiently Eliminates Colorectal Cancer Stem Cells. *Cancer Res.* 2019;79(7):1426-37.
37. He K, Sun H, Zhang J, Zheng R, Gu J, Luo M, et al. Rab7-mediated autophagy regulates phenotypic transformation and behavior of smooth muscle cells via the Ras/Raf/MEK/ERK signaling pathway in human aortic dissection. *Mol Med Rep.* 2019;19(4):3105-13.
38. Dalvi P, Sharma H, Chinnappan M, Sanderson M, Allen J, Zeng R, et al. Enhanced autophagy in pulmonary endothelial cells on exposure to HIV-Tat and morphine: Role in HIV-related pulmonary arterial hypertension. *Autophagy.* 2016;12:2420-38.
39. Gomez-Puerto M, van Zuijen I, Huang C, Szulcek R, Pan X, van Dinther M, et al. Autophagy contributes to BMP type 2 receptor degradation and development of pulmonary arterial hypertension. *J Pathol.* 2019;249(3):356-67.
40. Haslip M, Dostanic I, Huang Y, Zhang Y, Russell K, Jurczak M, et al. Endothelial uncoupling protein 2 regulates mitophagy and pulmonary hypertension during intermittent hypoxia. *Arterioscler Thromb Vasc Biol.* 2015;35(5):1166-78.
41. Masri F, Xu W, Comhair S, Asosingh K, Koo M, Vasanji A, et al. Hyperproliferative apoptosis-resistant endothelial cells in idiopathic pulmonary arterial hypertension. *Am J Physiol Lung Cell Mol Physiol.* 2007;293(3):L548-54.
42. Toshner M, Voswinckel R, Southwood M, Al-Lamki R, Howard L, Marchesan D, et al. Evidence of dysfunction of endothelial progenitors in pulmonary arterial hypertension. *Am J Respir Crit Care Med.* 2009;180(8):780-7.
43. Ranchoux B, Antigny F, Rucker-Martin C, Hautefort A, Pechoux C, Bogaard HJ, et al. Endothelial-to-Mesenchymal Transition in Pulmonary Hypertension. *Circulation.* 2015;131(11):1006-18.
44. Hopper R, Moonen J, Diebold I, Cao A, Rhodes C, Tojais N, et al. In Pulmonary Arterial Hypertension, Reduced BMPR2 Promotes Endothelial-to-Mesenchymal Transition via HMGA1 and Its Target Slug. *Circulation.* 2016;133(18):1783-94.

45. Good RB, Gilbane AJ, Trinder SL, Denton CP, Coghlan G, Abraham DJ, et al. Endothelial to Mesenchymal Transition Contributes to Endothelial Dysfunction in Pulmonary Arterial Hypertension. *Am J Pathol.* 2015;185(7):1850-8.
46. Santarelli R, Arteni AMB, Gilardini Montani MS, Romeo MA, Gaeta A, Gonnella R, et al. KSHV dysregulates bulk macroautophagy, mitophagy and UPR to promote endothelial to mesenchymal transition and CCL2 release, key events in viral-driven sarcomagenesis. *Int J Cancer.* 2020;147(12):3500-10.
47. Hariharan N, Maejima Y, Nakae J, Paik J, Depinho R, and Sadoshima J. Deacetylation of FoxO by Sirt1 Plays an Essential Role in Mediating Starvation-Induced Autophagy in Cardiac Myocytes. *Circ Res.* 2010;107(12):1470-82.
48. Dorayappan K, Wanner R, Wallbillich J, Saini U, Zingarelli R, Suarez A, et al. Hypoxia-induced exosomes contribute to a more aggressive and chemoresistant ovarian cancer phenotype: a novel mechanism linking STAT3/Rab proteins. *Oncogene.* 2018;37(28):3806-21.
49. Li C, Fang Y, Wang K, Gao W, Dou Z, Wang X, et al. Protective effect of c-Myc/Rab7a signal pathway in glioblastoma cells under hypoxia. *Ann Transl Med.* 2020;8(6):283.
50. Surviladze Z, Ursu O, Miscioscia F, Curpan R, Halip L, Bologa C, et al. *Probe Reports from the NIH Molecular Libraries Program*. Bethesda (MD): National Center for Biotechnology Information (US); 2010.
51. Sakao S, Taraseviciene-Stewart L, Cool CD, Tada Y, Kasahara Y, Kurosu K, et al. VEGF-R blockade causes endothelial cell apoptosis, expansion of surviving CD34+ precursor cells and transdifferentiation to smooth muscle-like and neuronal-like cells. *FASEB J.* 2007;21(13):3640-52.
52. Roy SG, Stevens MW, So L, and Edinger AL. Reciprocal effects of rab7 deletion in activated and neglected T cells. *Autophagy.* 2013;9(7):1009-23.
53. Chen MJ, Yokomizo T, Zeigler BM, Dzierzak E, and Speck NA. Runx1 is required for the endothelial to haematopoietic cell transition but not thereafter. *Nature.* 2009;457(7231):887-91.
54. Farkas D, Thompson AAR, Bhagwani AR, Hultman S, Ji H, Kotha N, et al. Toll-like Receptor 3 Is a Therapeutic Target for Pulmonary Hypertension. *Am J Respir Crit Care Med.* 2019;199(2):199-210.
55. Urboniene D, Haber I, Fang Y, Thenappan T, and Archer S. Validation of high-resolution echocardiography and magnetic resonance imaging vs. high-fidelity catheterization in experimental pulmonary hypertension. *Am J Physiol Lung Cell Mol Physiol.* 2010;299(3):L401-12.

FIGURES

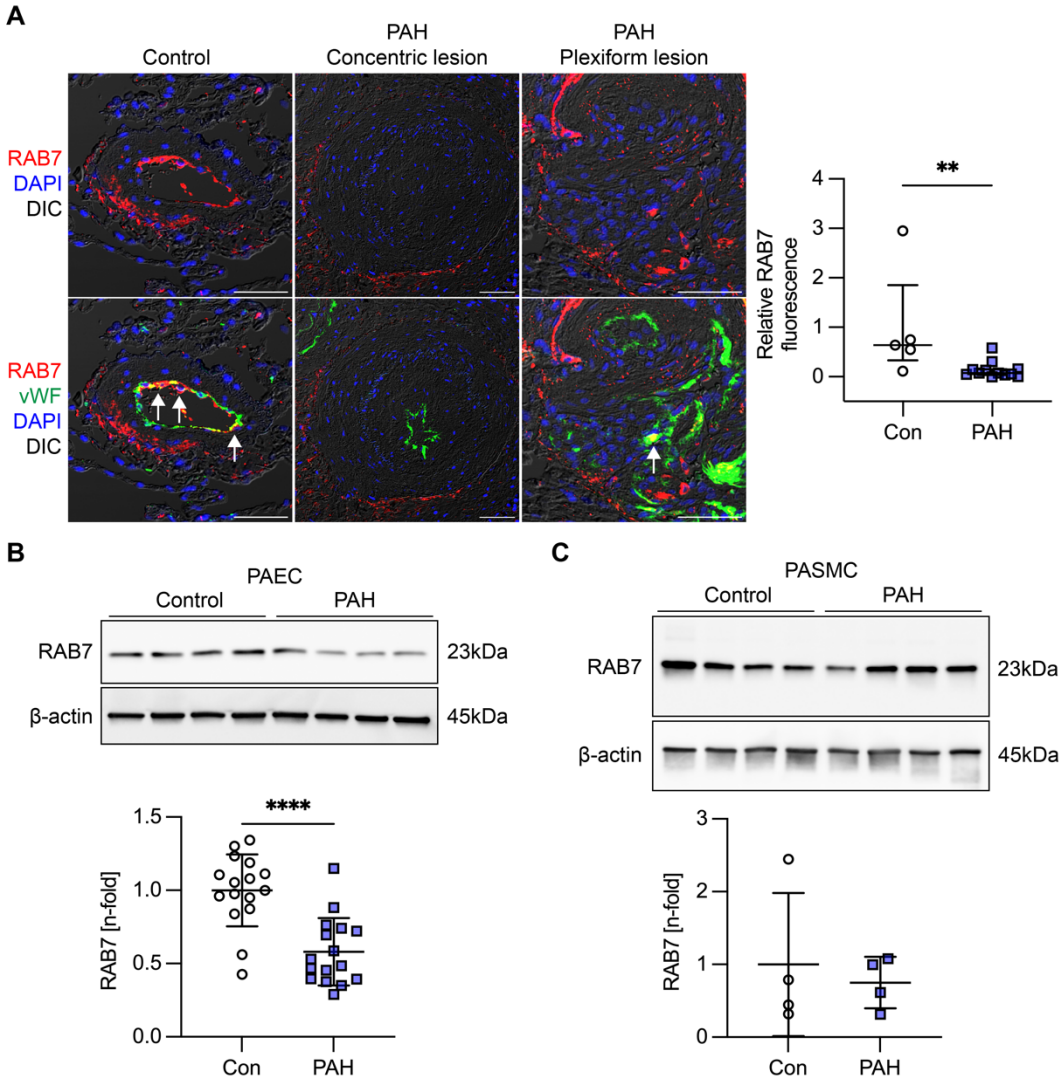

Figure 1. Reduced RAB7 expression in endothelial cells from PAH patients. (**A**) Representative optical sections (confocal microscopy, representative of n=5 pulmonary arteries from n=3 control patients and n=12 pulmonary arteries from n=3 PAH patients) show reduced RAB7 expression in ECs in concentric and plexiform lesions from PAH patients compared to controls. Arrows indicate vWF^{+} ECs with strong RAB7 expression. Scale bar: 50µm. Nuclear staining with DAPI. The graph shows quantification of relative RAB7 immunofluorescence in ECs from control and PAH pulmonary arteries. (**B-C**) Representative Immunoblot (n=4 individual control and PAH PAEC lines) and quantification of RAB7 in PAECs (B) in 4 immunoblots from n=12 individual control (failed donor) and n=15 individual PAH patients (n=16 data points total per each group due to 4 repeat experiments). (C) shows representative immunoblot and quantification of RAB7 in PASMCs from n=4 individual control (failed donor) and n=4 individual PAH patients. β-actin is shown as loading control. All graphs show single values and median ± interquartile

rank (A) or mean ± SD (B, C). The data were compared using a 2-tailed Mann-Whitney test (A) or a 2-tailed Student's t-test (B, C). **P<0.01, ****P<0.0001.

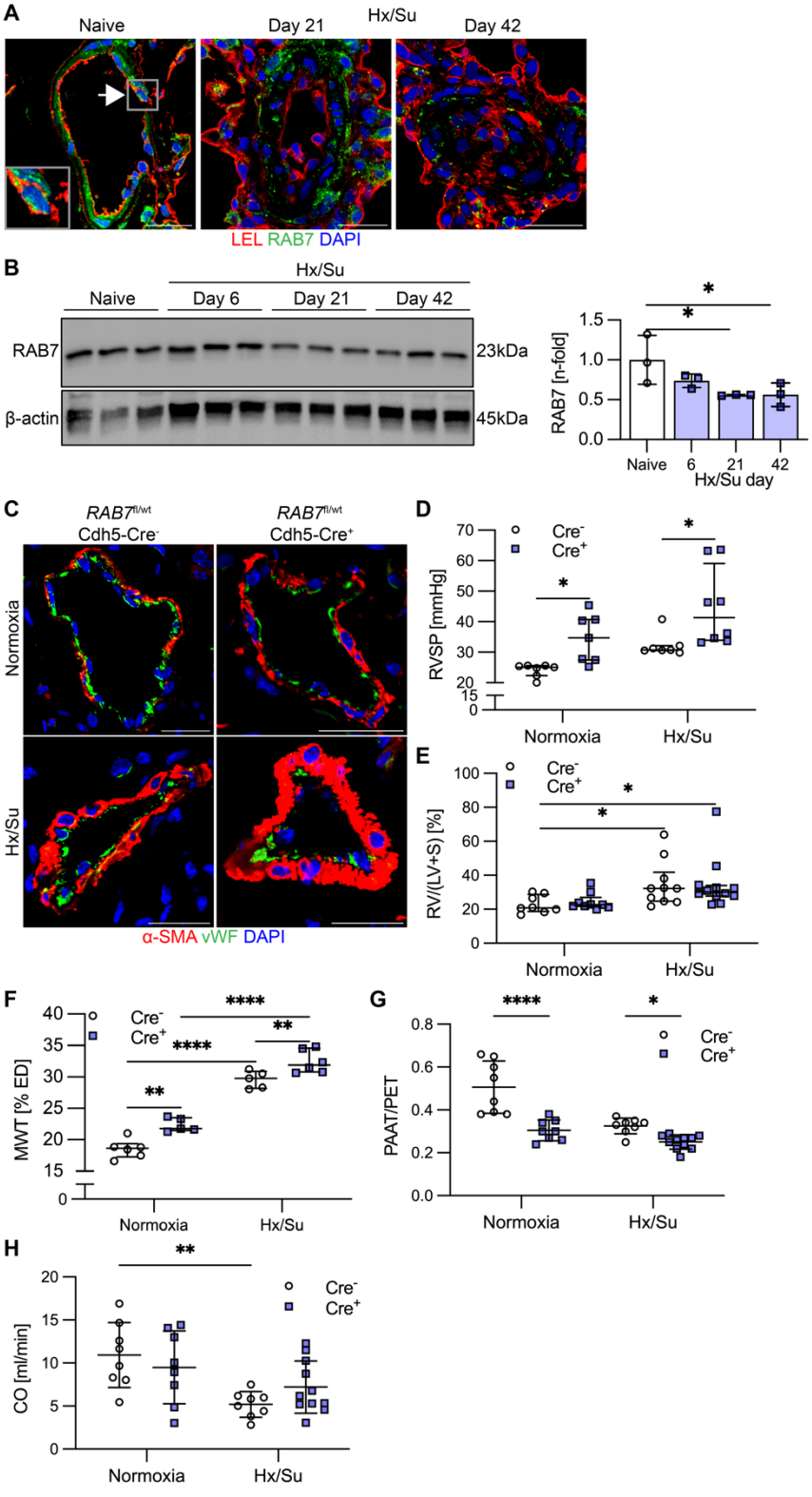

Figure 2. Loss of RAB7 expression causes PH in vivo. (**A**) Representative immunofluorescence images (representative of n=3) (confocal microscopy) show strong RAB7 staining (green pseudocolor) in pulmonary arteries (PAs) from naïve rats, including

in PAECs (representative cell indicated by arrow and shown in more detail in insert) (PAEC indicated by Lysopersicon esculentum, Tomatolectin, LEL, staining, red pseudocolor). In chronic hypoxia + SU5416 (Hx/Su) treated rats, RAB7 expression decreased in ECs in the remodeled PAs at days 21 and 42. Scale bars: 25 µm. (**B**) Representative immunoblot and densitometry of RAB7 expression in naïve and Hx/Su rats. (**C**) Representative double immunofluorescence for von Willebrand Factor (vWF) and α-smooth muscle actin (α-SMA) (optical section, confocal microscopy). Scale bars: 25 µm. (**D-H**) Right ventricular systolic pressure (RVSP, D), Fulton RV hypertrophy index [RV/(left ventricle+Septum)] (E), pulmonary artery media wall thickness (MWT, F), pulmonary artery acceleration time vs. pulmonary ejection time ratio (PAAT/PET, G), echocardiographically estimated cardiac output (CO, H) of *RAB7*$^{fl/wt}$ Cdh5-Cre^{-} and *RAB7*$^{fl/wt}$ Cdh5-Cre^{+} mice exposed to normoxia and Hx/Su. n numbers: n=3 per group (B), (D) n=7, except n=8 for Hx/Su Cre^{+}. (E) n=8, except n=9 (normoxia Cre^{+}), n=10 (Hx/Su Cre^{-} and n=12 (Hx/Su Cre^{+}). (F) n=5 (normoxia Cre^{+} and Hx/Su Cre^{-}), n=6 (normoxia Cre^{-} and Hx/Su Cre^{+}). (G, H) n=8, except n=12 (Hx/Su Cre^{+}). Data were compared using One-Way ANOVA followed by Holm-Sidak multiple comparison test (B), Two-way ANOVA with Holm-Sidak multiple comparison test, and evaluation of normality of residual distribution (D'Agostino-Pearson) (D, F), and Kruskal-Wallis Analysis with Dunn's multiple comparison test (E). All graphs show single values and mean ± SD (B, F, G, H) or median ± interquartile rank (D, E). *P<0.05, **P<0.01, ****P<0.0001.

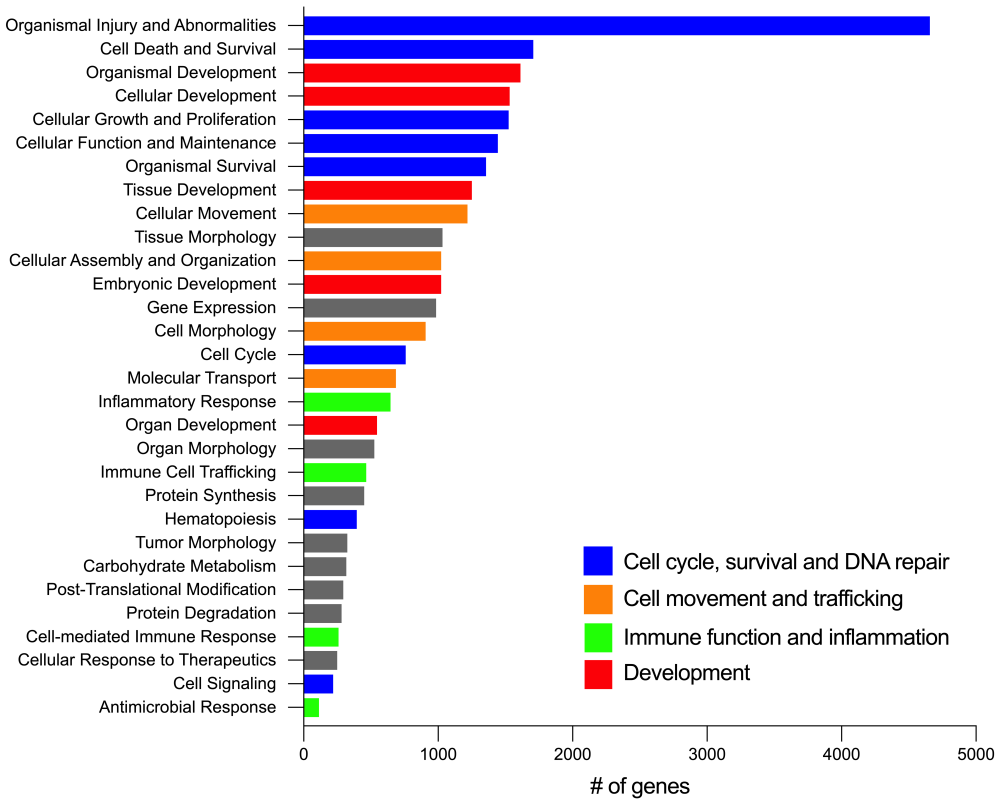

Figure 3. RNA sequencing of *RAB7* silenced pulmonary artery ECs. Ingenuity pathway analysis of bulk RNA sequencing data in PAECs transfected with *RAB7* siRNA vs. control siRNA (fold change >|1.25|, adjusted P value <0.05) (representing n=3 per group). The diagram shows the 30 most regulated function terms showing the number of differentially expressed genes (DEG) in the RNAseq dataset within each category. DEG terms were labeled according to their relevance for cell cycle and DNA repair (blue), cellular movement and trafficking (orange), immune function and inflammation (green), and development (red).

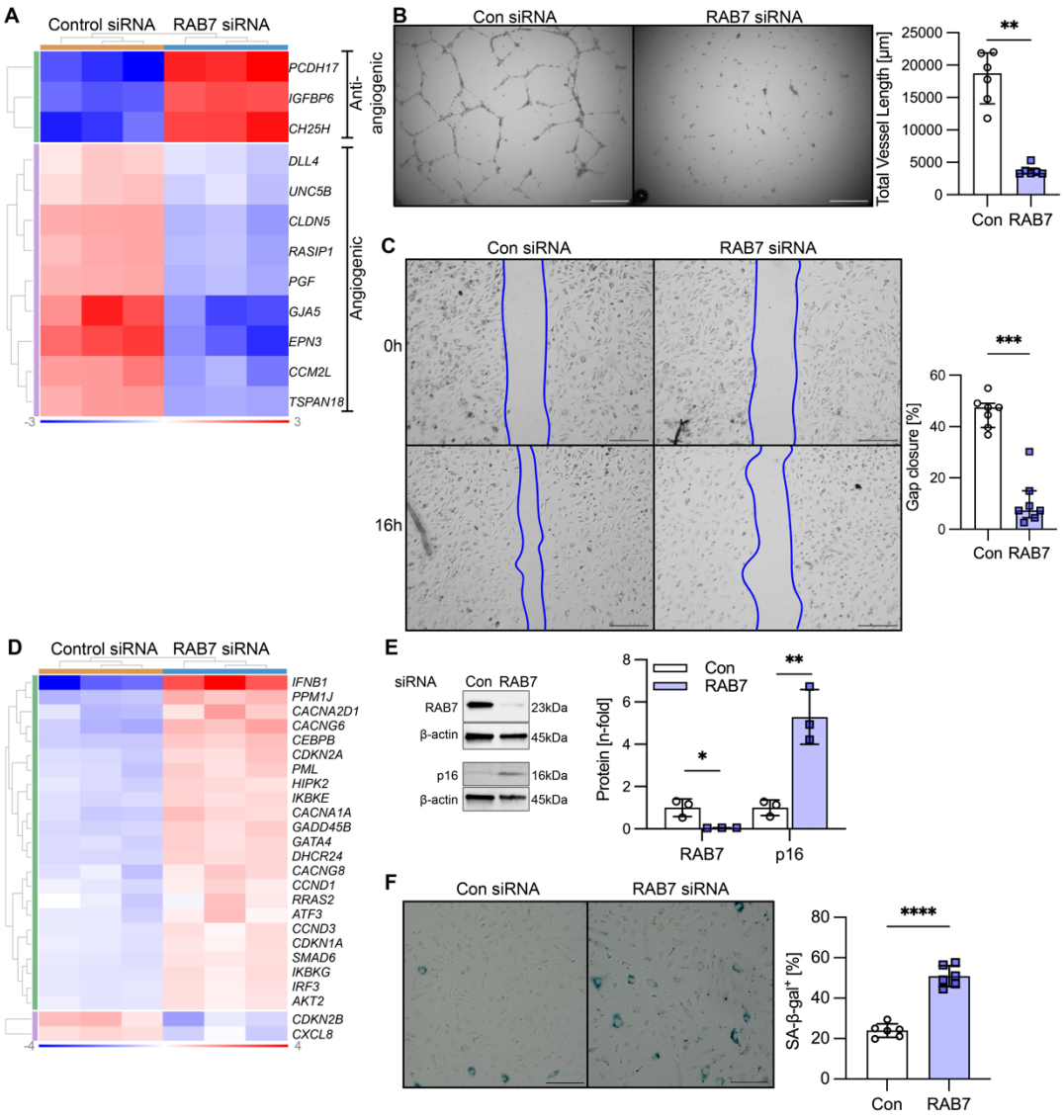

Figure 4. Loss of RAB7 induces endothelial dysfunction and senescence in pulmonary artery ECs. (**A**) The clustered heatmap demonstrates increased expression of anti-angiogenic genes, and reduced expression of angiogenic and EC barrier function genes in RNAseq of PAECs after *RAB7* siRNA treatment vs. control siRNA. n=3 per group. (**B**) Representative phase contrast images after 24h and quantification of total network length in *RAB7* siRNA treated PAECs. n=6 per group. (**C**) Representative phase contrast after 16h of gap closure assay and quantification of percent gap closure in *RAB7* siRNA transfected PAECs vs. control siRNA. n=7 per group. (**D**) Clustered heatmap of DEGs of senescence-associated gene expression pattern (Ingenuity Pathway Analysis) in RNAseq of PAECs treated with *RAB7* siRNA. n=3 per group. (**E**) Representative immunoblots and densitometric quantification for RAB7 and p16 in PAECs treated with *RAB7* siRNA. n=3 per group. (**F**) Representative images and quantification of the fraction of SA-β-gal$^+$ PAECs after *RAB7* siRNA treatment vs. control siRNA. n=6 per group. Data are shown as single values and median ± interquartile rank (B, C) or mean ± SD (E, F). Data were analyzed using 2-tailed Mann-Whitney test (B, C) or 2-tailed Student's t-test

(E, F). Heatmap data is normalized log_2 fold expression. Data in B, C, E, F are representative of n≥2 experiments. Scale bars: 200 μm (F), 250 μm (B, C). *P<0.05, **P<0.01, ***P<0.001, ****P<0.0001.

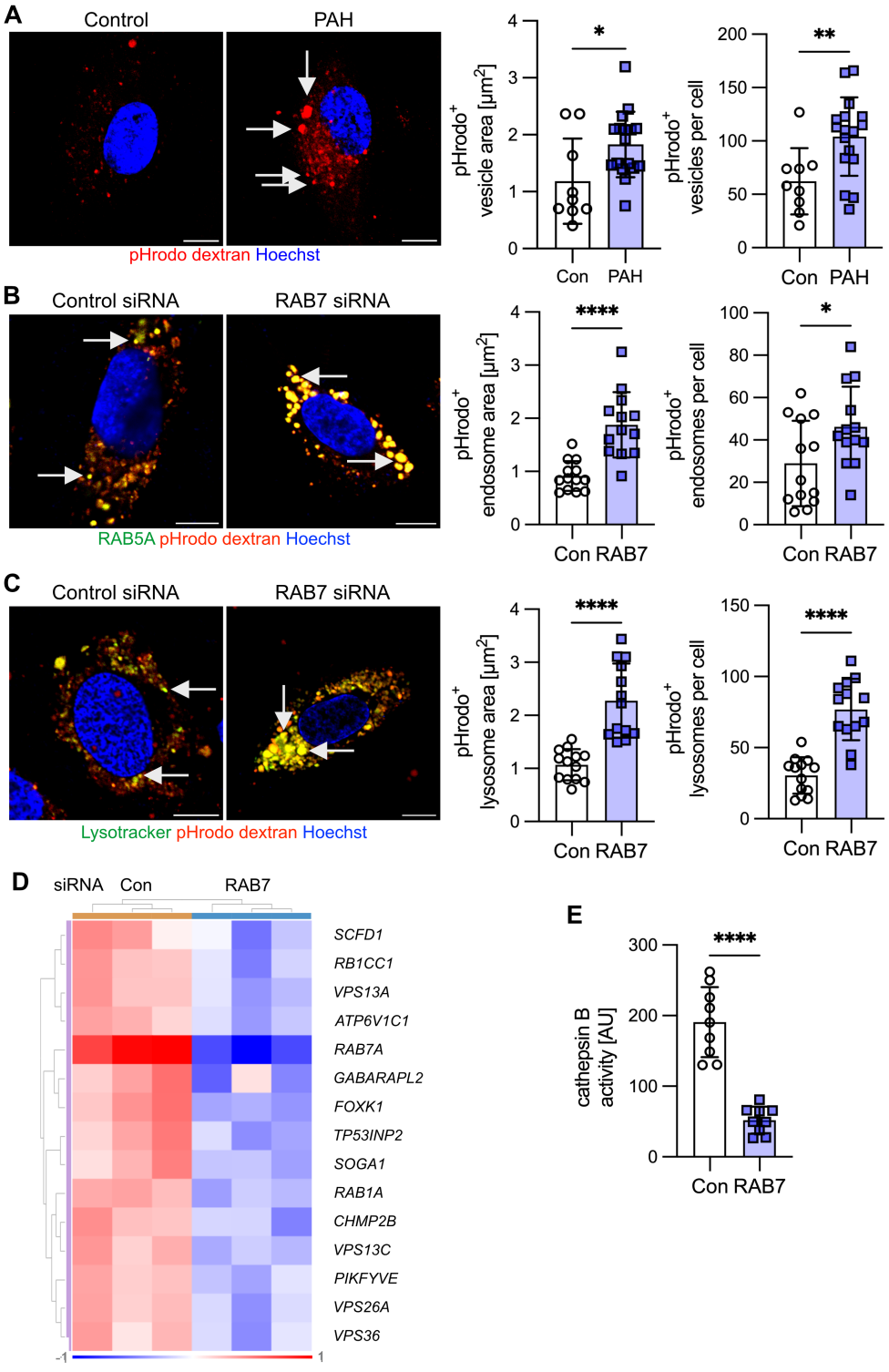

Fig. 5. Impaired endosome-lysosome function in PAH pulmonary artery ECs and RAB7 deficient pulmonary artery ECs. (**A**) Representative optical sections (confocal microscopy) and quantification of pHrodo dextran$^+$ vesicle area and number of vesicles per cell indicate accumulation of pHrodo dextran after 20 min in enlarged vesicles in PAH PAECs (arrows), but not in control PAECs (Con). pHrodo dextran is taken up by

endosomes and emits red fluorescence signal when pH drops during endosomal acidification. n=9 (control) and n=17 (PAH). (**B**) Representative optical sections (confocal microscopy) show an accumulation of pHrodo dextran after 20 min. in enlarged early endosomes with *RAB7* silencing. Early endosomes were identified by transfection of PAECs with baculovirus expressing GFP-labeled RAB5. Quantification of $RAB5^+$ pHrodo $dextran^+$ endosome area and number per cell confirms that dextran accumulates in enlarged early endosomes following RAB7 silencing. n=13 per group. (**C**) Representative optical sections (confocal microscopy) show an accumulation of pHrodo dextran after 20 min. in enlarged lysosomes in *RAB7* siRNA-treated PAECs. Lysosomes were labeled with lysotracker. Quantification of $lysotracker^+$ pHrodo $dextran^+$ lysosome area and number per cell confirms that dextran accumulates in enlarged lysosomes following RAB7 silencing. n=13 per group. (**D**) The clustered heatmap shows autophagy-related DEG that was found to be downregulated in RNAseq from PAECs treated with *RAB7* siRNA. Expression as normalized log_2 fold. (**E**) Reduced cathepsin B activity also indicates impaired lysosomal autophagy. n=9 per group. Scale bars: 10 μm. In (A) Con indicates control PAECs, in (B-E) Con indicates control siRNA. All graphs show single values and mean ± SD. Data in A-C are representative of n≥2 experiments. Data were analyzed using 2-tailed Student's t-test. *P<0.05, **P<0.01, ****P<0.0001.

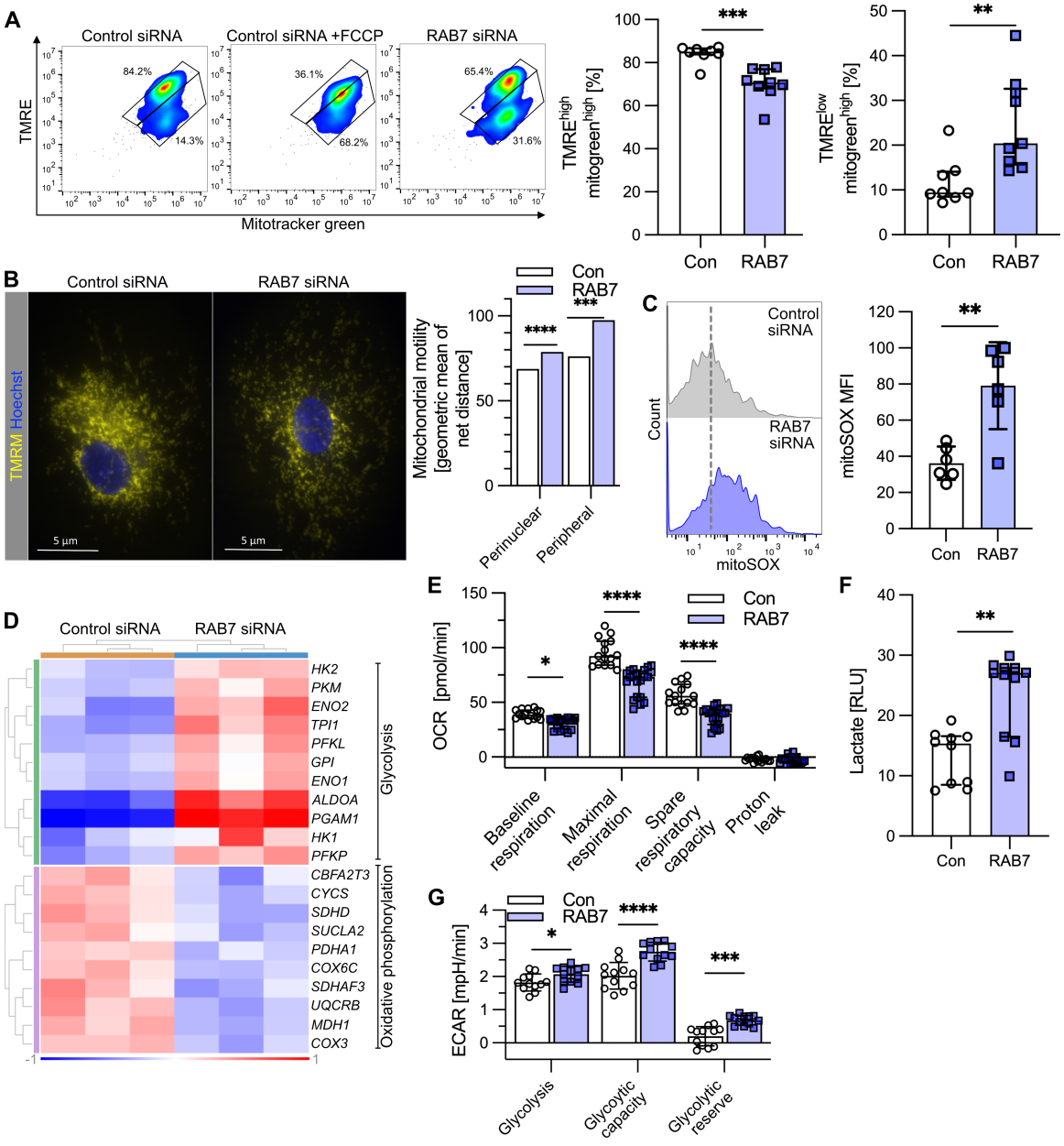

Fig. 6 *RAB7* silencing impairs mitochondrial membrane potential and mitochondrial function. (**A**) *RAB7* siRNA impairs $\Delta\Psi_m$ as assessed by TMRE and mitotracker green (mitogreen) flow cytometry. Carbonyl cyanide p-trifluoro methoxyphenylhydrazone (FCCP) is a positive control (depolarizes mitochondrial membrane). $TMRE^{high}$ $mitogreen^{high}$ cells indicate cells with functional mitochondria, whereas $TMRE^{low}$ $mitogreen^{high}$ cells are cells with dysfunctional mitochondria. n=8 (con) and n=9 (RAB7). (**B**) Representative TMRM staining images show overall reduction and perinuclear accumulation of functional mitochondria in *RAB7* siRNA. Representative of n=3 experiments. Scale bar: 5 µm. *RAB7* knockdown increases mitochondrial motility in the peripheral and the perinuclear regions. (**C**) *RAB7* knockdown promotes mitochondrial ROS production as indicated by flow cytometry for mitoSOX. n=6 per group,

representative histogram plots, and quantification of MFI. (**D**) Clustered heatmap: upregulated glycolysis-related DEGs and downregulated oxidative phosphorylation-related DEGs in bulk RNAseq from PAECs + RAB7 siRNA. Expression: normalized log_2 fold. (**E**) Seahorse high-resolution respirometrics show reduced oxygen consumption rate (OCR) with *RAB7* siRNA at basal respiration, maximal respiration, and spare respiratory capacity. N=15 (con) and n=21 (RAB7). (**F**) Luminescence assay for lactate: increased lactate production in RAB7 siRNA. n=10 (control, con) and n=11 (RAB7). (**G**) Extracellular acidification rate (ECAR) data show more rapid acidification (i.e., greater reliance on glycolysis) in the RAB7 siRNA PAECs as shown for glycolysis, basal and maximum glycolytic rate. n=12 per group. All graphs show single values and median ± interquartile range (A, E, F) or mean ± SD (C, G) (except B, as bar graphs in B indicate the geometric mean of a log-normal distribution). Data in A, B, C, E, F, and G are from n≥2 experiments. Data were analyzed using 2-tailed Mann-Whitney test (A, F), 2-tailed Student's t-test (C) and 2-way ANOVA (E, G) with Holm-Sidak post-hoc test and normality testing of residuals (D'Agostino-Pearson). *P<0.05, **P<0.01, ***P<0.001 and ****P<0.0001.

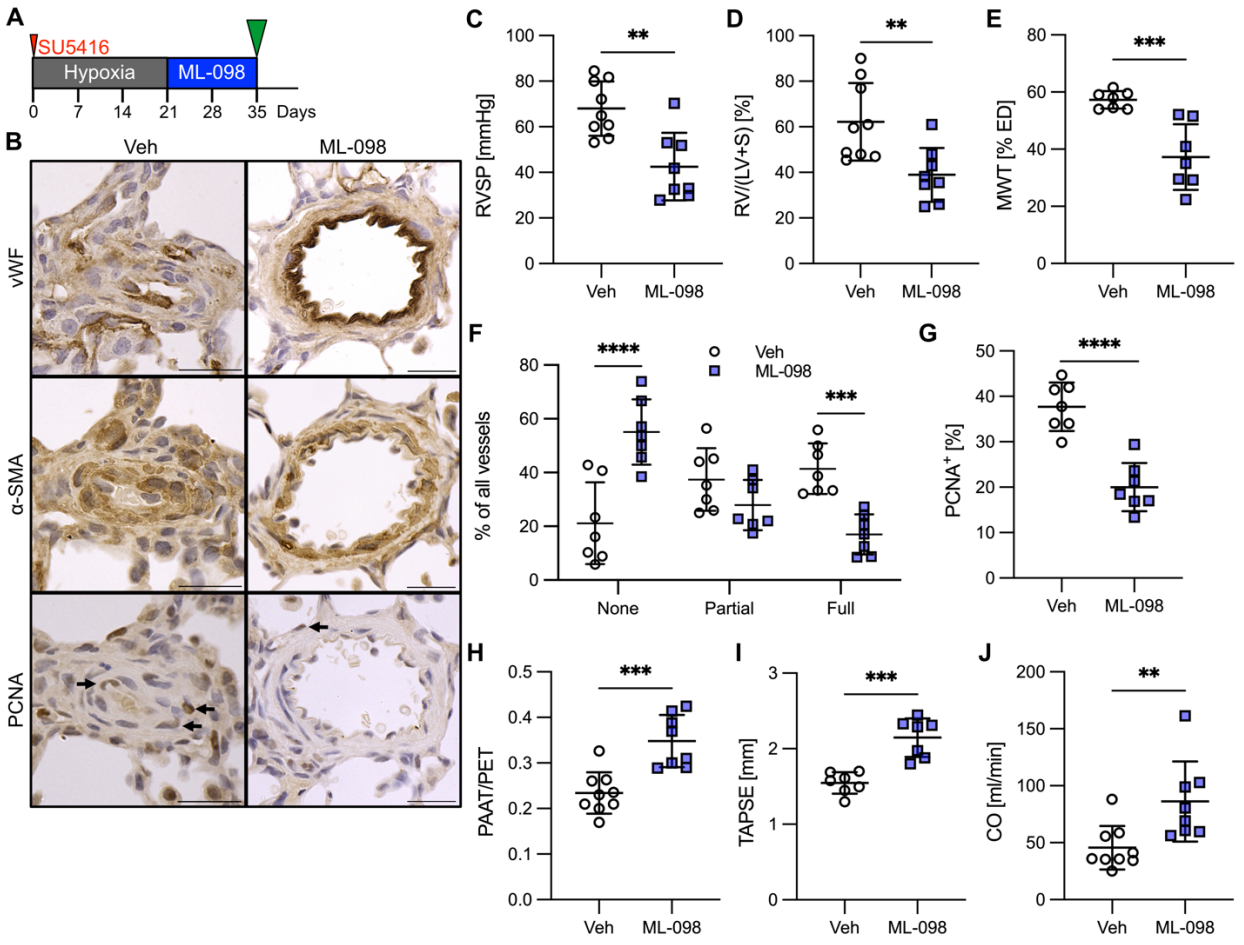

Figure 7. RAB7 activator ML-098 reduces PH in rats exposed to chronic hypoxia/SU5416. (**A**) interventional treatment diagram. (**B**) Representative vWF, α-SMA and PCNA immunohistochemistry showing serial sections of the same pulmonary artery. (**C**) RVSP, (**D**) Fulton index, (**E**) MWT of small pulmonary arteries, (**F**) occlusion of small pulmonary arteries, (**G**) percentage of PCNA$^+$ pulmonary artery mural cells, (**H**) ratio of pulmonary artery acceleration time (PAAT) vs. pulmonary ejection time (PET), (**I**) tricuspid annular plane systolic excursion (TAPSE) and (**J**) echocardiographic estimation of right ventricular cardiac output (CO). Scale bars: 25 µm. n=9 (veh) and n=8 (ML-098) (C, D, H, J), n=7 (E, F, G, I). All graphs show single values and mean ± SD. Data were analyzed using 2-sided Student's t-test. **P<0.01, ***P<0.001, ****P<0.0001.

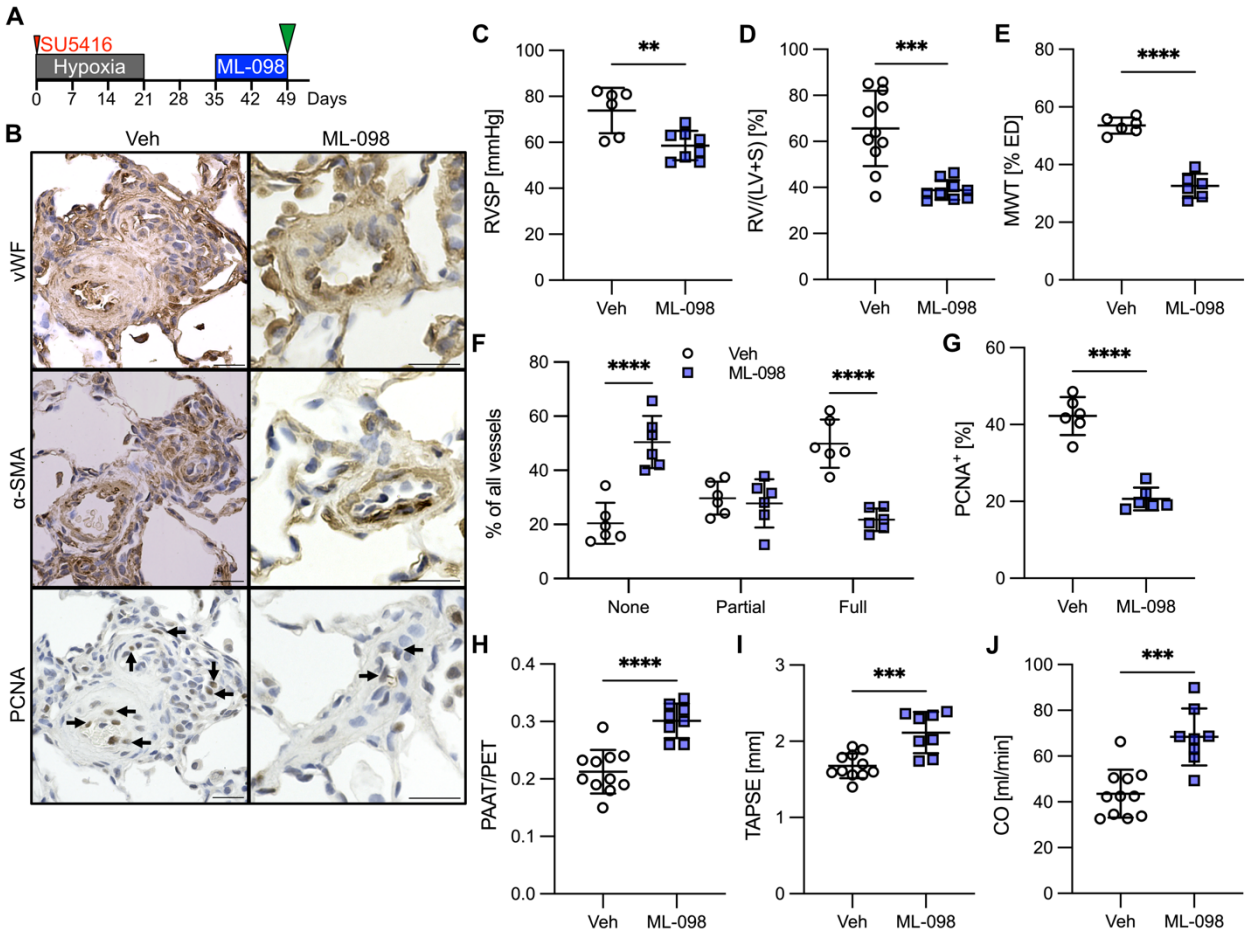

Figure 8. RAB7 activator ML-098 reverses established PH in rats exposed to chronic hypoxia/SU5416. (**A**) Reversal treatment diagram. (**B**) Representative vWF, α-SMA, and PCNA immunohistochemistry showing serial sections of the same pulmonary artery. (**C**) RVSP, (**D**) Fulton index, (**E**) MWT of small pulmonary arteries, (**F**) occlusion of small pulmonary arteries, (**G**) percentage of PCNA$^+$ pulmonary artery mural cells, and echocardiography data for (**H**) ratio of pulmonary artery acceleration time (PAAT) vs. pulmonary ejection time (PET), (**I**) tricuspid annular plane systolic excursion (TAPSE) and (**J**) right ventricular cardiac output (CO). Scale bars: 25 μm. n=6 (veh) and n=8 (ML-098) (C), n=11 (veh) and n=9 (ML-098) (D), n=6 (E-G), n=11 (veh) and n=8 (ML-098) (H-J). All graphs show single values and mean ± SD. Data were analyzed using 2-sided Student's t-test. **P<0.01, ***P<0.001, ****P<0.0001.